

# The 10.5 year rotation period of the strongly magnetic rapidly oscillating Ap star HD 166473<sup>★</sup>

G. Mathys<sup>1</sup>, V. Khalack<sup>2</sup>, and J. D. Landstreet<sup>3,4</sup>

<sup>1</sup> European Southern Observatory, Alonso de Cordova 3107, Vitacura, Santiago, Chile  
e-mail: gmathys@eso.org

<sup>2</sup> Département de Physique et d'Astronomie, Université de Moncton, Moncton, NB, Canada E1A 3E9

<sup>3</sup> Department of Physics & Astronomy, University of Western Ontario, 1151 Richmond Street, London, Ontario N6A 3K7, Canada

<sup>4</sup> Armagh Observatory, College Hill, Armagh, BT61 9DG, Northern Ireland, UK

Received ... / Accepted ...

## ABSTRACT

**Context.** How magnetic fields contribute to the differentiation of the rotation rates of the Ap stars and affect the occurrence of non-radial pulsation in some of them are important open questions. Valuable insight can be gained into these questions by studying some of the most extreme examples of the processes at play. The super-slowly rotating rapidly oscillating Ap (roAp) star HD 166473 is such an example.

**Aims.** We performed the first accurate determination of its rotation period,  $P_{\text{rot}} = (3836 \pm 30)$  d, from the analysis of 56 measurements of the mean magnetic field modulus  $\langle B \rangle$  based on high-resolution spectra acquired between 1992 and 2019 at various observatories and with various instrumental configurations.

**Methods.** We complemented this analysis with the consideration of an inhomogeneous set of 21 determinations of the mean longitudinal magnetic field  $\langle B_z \rangle$  spanning the same time interval.

**Results.** This makes HD 166473 one of only four Ap stars with a period longer than 10 years for which magnetic field measurements have been obtained over more than a full cycle. The variation curves of  $\langle B \rangle$  and of  $\langle B_z \rangle$  are well approximated by cosine waves. The magnetic field of HD 166473 only seems to deviate slightly from axisymmetry, but it definitely involves a considerable non-dipolar component.

**Conclusions.** Among the stars with rotation periods longer than 1000 d for which magnetic field measurements with full phase coverage are available, HD 166473 has the strongest field. Its magnetic field is also one of the strongest known among roAp stars. Overall, the magnetic properties of HD 166473 do not seem fundamentally distinct from those of the faster-rotating Ap stars. However, considering as a group the eight Ap stars that have accurately determined periods longer than 1000 d and whose magnetic variations have been characterised over a full cycle suggests that the angles between their magnetic and rotation axes tend to be systematically large.

**Key words.** Stars: individual: HD 166473 – Stars: chemically peculiar – Stars: rotation – Stars: magnetic field – Stars: oscillations

## 1. Introduction

The existence of a sizeable population of Ap stars that rotate extremely slowly is now well established. According to Mathys (2017), stars with rotation periods ( $P_{\text{rot}}$ ) longer than one year may represent several percent of all Ap stars. At present, at least 20 Ap stars that definitely have  $P_{\text{rot}} > 1$  yr are known. But statistical arguments indicate with a high level of confidence that there exist many more Ap stars with such long periods.

Consideration of the extremely slowly rotating Ap stars is important to understand the origin and the evolution of the rotational properties of Ap stars as a class, and more generally, of all upper main sequence stars. Within that context, identifying de-

pendencies or correlations between the rotation rates and other properties of these stars can potentially provide very valuable insight. As an example of such a correlation, Mathys et al. (1997) reported that very strong magnetic fields ( $\langle B \rangle_{\text{av}} \gtrsim 7.5$  kG) are found only in stars with rotation periods shorter than  $\sim 150$  days. This result was subsequently confirmed, at a very high level of significance, by Mathys (2017). The notation  $\langle B \rangle_{\text{av}}$  denotes the average over a stellar rotation cycle of the mean magnetic field modulus ( $\langle B \rangle$ , the line-intensity weighted average over the visible stellar disk of the modulus of the magnetic vector).

Until now, magnetic field measurements covering more than a full rotation cycle with adequate sampling have been obtained for seven of the 20 Ap stars known to have a rotation period longer than one year. Such a complete phase coverage is essential to characterise the main properties of the stellar magnetic field, including its geometric structure. This characterisation is required to identify possible correlations between the rotation rate, the magnetic field, and other physical properties (e.g., mass, age, abundance anomalies and inhomogeneities) of the Ap stars.

With regard to the connection between rotation and other physical properties, the situation of the rapidly oscillating Ap (roAp) stars is particularly intriguing. Of the 61 roAp stars in-

<sup>★</sup> Based on observations collected at the Canada-France-Hawaii Telescope (CFHT), which is operated by the National Research Council of Canada, the Institut National des Sciences de l'Univers of the Centre National de la Recherche Scientifique of France, and the University of Hawaii; and on data products from observations made with ESO Telescopes at the La Silla Paranal Observatory under programmes 79.C-0170, 80.C-0032, 81.C-0034, and 89.D-0383. The operations at the Canada-France-Hawaii Telescope are conducted with care and respect from the summit of Mauna Kea, which is a significant cultural and historic site.

ventoried by Smalley et al. (2015), 14 show spectral lines resolved into their magnetically split components (see Tables 1 and 2 of Mathys 2017). In other words, the rate of occurrence of magnetically resolved lines in roAp stars seems significantly higher than average – no more than a few percent of all Ap stars. While a few of the Ap stars with resolved magnetically split lines may be short period stars whose rotation axis has a low inclination to the line of sight, most of them are genuine slow rotators (Mathys 2017). This suggests that slow rotators may also be more frequent among roAp stars than among Ap stars in general. As a matter of fact, of the 14 roAp stars with resolved magnetically split lines, nine definitely have, or may plausibly have, a rotation period longer than one year. Furthermore, at least two of the roAp stars with unresolved lines are also suspected to have  $P_{\text{rot}} > 1$  yr: HD 101065 (Przybylski’s star), for which Hubrig et al. (2018) proposed a tentative, extrapolated value  $P_{\text{rot}} \approx 188$  yr, and HD 176232 (= 10 Aql), for which Mathys & Lanz (1992) suggested that the period might be of the order of years, and Pyper & Adelman (2017) did not detect any photometric variation over a time interval of 12 years. Based on these considerations, it is not implausible that more than 15% of the roAp stars could have rotation periods in excess of one year – a strikingly high fraction compared to the rate of occurrence of extremely slow rotation in the entire population of Ap stars. Whether this high fraction is indicative of a direct connection between slow rotation and the occurrence of non-radial pulsation, or if it results from independent links between each of those two features and other physical parameters of the stars where both occur simultaneously (such as the mass) remains to be elucidated.

Within this context, the A5p SrCrEu star (Renson & Manfroid 2009) HD 166473 (= V694 CrA) is a particularly interesting specimen in several respects. Kurtz & Martinez (1987) discovered that HD 166473 is a roAp star, showing low amplitude photometric variations with periods between 8.8 and 9.1 min. Mathys et al. (1997) reported the observation of resolved magnetically split lines in the spectrum of this star. The first measurements of its mean longitudinal magnetic field ( $\langle B_z \rangle$ , the line intensity weighted average over the stellar disk of the component of the magnetic vector along the line of sight) were carried out by Mathys & Hubrig (1997). Kurtz et al. (2003) reported observations of radial velocity variations with the pulsation frequencies, which were analysed in greater detail by Mathys et al. (2007). These authors presented additional measurements of the mean magnetic field modulus, and combined them with determinations of other magnetic field moments (which were eventually published by Mathys 2017) to infer that the rotation period of HD 166473 must be of the order of 10 yr. More recently, Shavrina et al. (2014) reported a value of  $P_{\text{rot}} = 3514$  d for the rotation period. This value appears to have been estimated from the measurements published by Mathys et al. (2007), which span a time base of 3631 d, and from six additional determinations of  $\langle B \rangle$ , derived from spectra recorded at unspecified epochs spread over a time interval of similar length.

From the studies listed above, it definitely emerges that the rotation period of HD 166473 cannot be significantly shorter than 10 yr and that this star has a strong magnetic field, with a value of the order of 7 kG for the average of the mean magnetic field modulus over a rotation cycle. This field strength locates it very close to the upper limit that was identified for the fields of Ap stars with rotation periods longer than  $\sim 150$  d. Moreover, among the roAp stars, until now, stronger fields have only been observed in two: HD 154708 (24.5 kG, Kurtz et al. 2006) and

HD 92499 (8.2 kG, Elkin et al. 2010). This is significant with respect to the relationship between the magnetic field and pulsation in roAp stars. For a description of the multiple facets of this relationship, see e.g. Kurtz et al. (2006).

Thus, in terms of its field strength, HD 166473 is one of the most extreme examples both of the population of super-slowly rotating Ap stars and of the class of the roAp stars. In many physical contexts, such extreme examples are known to provide very valuable insight into the processes at play. This represents a strong motivation to study HD 166473 in detail.

Here we present new determinations of the mean magnetic field modulus and of the mean longitudinal magnetic field of HD 166473, based on both dedicated observations and archive spectra. We derived for the first time an accurate value of the rotation period of the star from the complete set of existing  $\langle B \rangle$  measurements. The observational data and their analysis are presented in Sect. 2, and the determination of the stellar rotation period is described in Sect. 3. In Sect. 4, we discuss the constraints that the available magnetic data set on the field geometry, and related surface inhomogeneities. Finally, we consider the implications of the results of this analysis of HD 166473 within the contexts of Ap star rotation and pulsation.

## 2. Observations and data analysis

### 2.1. Mean magnetic field modulus

All the mean field modulus values used in this analysis were determined from the measured wavelength separation of the two magnetically split components of the Fe II  $\lambda$  6149.2 Å diagnostic line. The following formula was applied to derive  $\langle B \rangle$ :

$$\lambda_r - \lambda_b = g \Delta\lambda_Z \langle B \rangle. \quad (1)$$

In this equation,  $\lambda_r$  and  $\lambda_b$  are, respectively, the wavelengths of the red and blue split line components;  $g$  is the Landé factor of the split level of the transition ( $g = 2.70$ ; Sugar & Corliss 1985);  $\Delta\lambda_Z = k \lambda_0^2$ , with  $k = 4.67 \cdot 10^{-13} \text{ Å}^{-1} \text{ G}^{-1}$ ;  $\lambda_0 = 6149.258 \text{ Å}$  is the nominal wavelength of the considered transition.

As in many other Ap stars, the Fe II  $\lambda$  6149.2 Å line in HD 166473 is blended on the blue side with an unidentified rare earth line. However, this blend is less severe than in other stars, so that its impact on the precision and uniformity of the  $\langle B \rangle$  measurements does not represent a major concern (see below). In particular, it does not introduce any significant ambiguity in the combination of past measurements with new ones, unlike in the case of HD 965 (Mathys et al. 2019b). Thus, the present analysis makes use of the following published measurements of the mean magnetic field modulus of HD 166473: 23 measurements from Mathys et al. (1997), ten measurements from Mathys (2017), and seven additional measurements from Mathys et al. (2007). These measurements were obtained with six different instrumental configurations. Five of these configurations were described by Mathys (2017); for the sake of simplicity, we use the same symbols as this author to identify them in Fig. 2. One measurement of Mathys et al. (2007) was based on a spectrum recorded with the Very Long Camera (VLC) of the ESO Coudé Echelle Spectrograph (CES) fed by the ESO 3.6-m telescope (Dall 2005). This configuration is quite different from those used by Mathys et al. (1997) and Mathys (2017). This difference was overlooked by Mathys (2017).

Here, we present new  $\langle B \rangle$  data at additional epochs, from the analysis of the following high-resolution spectra recorded in natural light:

**Table 1.** Mean magnetic field modulus measurements.

JD	$\langle B \rangle$ (G)	Configuration
2448788.758	8551	ESO CAT + CES LC
2448790.817	8444	ESO CAT + CES LC
2448841.672	8454	ESO CAT + CES LC
2448911.512	8540	ESO CAT + CES LC
2449079.772	8412	ESO CAT + CES LC
2449100.913	8305	ESO CAT + CES LC
2449130.878	8138	ESO CAT + CES LC
2449160.832	8148	ESO CAT + CES LC
2449212.719	7991	ESO CAT + CES LC
2449215.670	7964	ESO CAT + CES LC
2449298.510	7878	ESO CAT + CES SC
2449301.510	7970	ESO CAT + CES SC
2449419.877	7645	ESO CAT + CES LC
2449437.843	7735	ESO CAT + CES SC
2449456.858	7552	ESO CAT + CES LC
2449494.717	7297	ESO CAT + CES LC
2449531.786	7341	ESO CAT + CES LC
2449793.849	6686	ESO CAT + CES LC
2449829.883	6651	ESO CAT + CES LC
2449853.877	6699	ESO CAT + CES LC
2449881.848	6680	ESO CAT + CES LC
2449908.774	6456	ESO CAT + CES LC
2449947.536	6395	ESO CAT + CES LC (lower res.)
2450132.885	5969	ESO CAT + CES LC
2450149.872	5883	ESO CAT + CES LC
2450171.896	5789	ESO CAT + CES LC
2450231.800	5820	ESO CAT + CES LC
2450522.835	5661	ESO CAT + CES LC
2450702.538	5770	ESO CAT + CES LC
2450900.853	6068	ESO CAT + CES LC
2450971.819	6095	ESO CAT + CES LC
2451042.606	6038	ESO CAT + CES LC
2451084.582	6118	ESO CAT + CES LC
2451326.017	6617	CFHT + Gecko
2451326.024	6623	CFHT + Gecko
2451600.858	7051	ESO 3.6 m + CES VLC
2451739.851	7565	CFHT + Gecko
2451740.863	7487	CFHT + Gecko
2452090.722	8450	ESO VLT UT2 + UVES
2452189.506	8349	ESO VLT UT2 + UVES
2452419.958	8790	CFHT + Gecko
2453214.889	7557	CFHT + Gecko
2454336.612	5748	ESO 3.6 m + HARPS
2454338.630	5709	ESO 3.6 m + HARPS
2454544.782	5761	ESO 3.6 m + HARPS
2454545.866	5754	ESO 3.6 m + HARPS
2454633.768	5745	ESO 3.6 m + HARPS
2454634.852	5766	ESO 3.6 m + HARPS
2454716.624	5794	ESO 3.6 m + HARPS
2456148.655	8518	ESO 3.6 m + HARPS
2456531.773	8540	CFHT + ESPaDOnS
2456547.732	8487	CFHT + ESPaDOnS
2456813.014	8203	CFHT + ESPaDOnS
2457239.836	7278	CFHT + ESPaDOnS
2457287.712	7170	CFHT + ESPaDOnS
2458642.993	5803	CFHT + ESPaDOnS

- one spectrum recorded with the Gecko spectrograph fed by the Canada-France-Hawaii Telescope (CFHT). This spectrum was reduced in the same way as previous spectra obtained with the same configuration (see Section 3 of Mathys et al. 1997 for details);

- six spectra recorded with the ESPaDOnS spectrograph fed by the Canada-France-Hawaii Telescope (CFHT). These spectra were reduced using the dedicated software package Libre-ESpRIT (Donati et al. 1997), which yields both the Stokes  $I$  spectrum and the Stokes  $V$  circular polarisation spectrum. The Stokes  $I$  spectra were normalised using the same procedure as in Khalack et al. (2017);
- one spectrum recorded with the Ultraviolet and Visible Echelle Spectrograph (UVES) fed by Unit Telescope 2 (UT2) of the ESO Very Large Telescope (VLT), retrieved from the ESO Archive;
- and eight spectra recorded with the High Accuracy Radial velocity Planet Searcher (HARPS) fed by the ESO 3.6-m telescope, retrieved from the ESO Archive. One of these spectra was obtained with the polarimetric mode of HARPS (HARPSpol; Piskunov et al. 2011) and is further discussed in Sect. 2.2.

For the HARPS and UVES observations, we used science grade pipeline processed data available from the ESO Archive. The only additional processing that we carried out was a continuum normalisation of the region ( $\sim 100 \text{ \AA}$  wide) surrounding the Fe II  $\lambda 6149.2 \text{ \AA}$  diagnostic line (except for the HARPSpol spectrum – see below).

The procedure actually used to measure the wavelengths  $\lambda_b$  and  $\lambda_r$  of the Fe II  $\lambda 6149.2 \text{ \AA}$  line is described in detail by Mathys & Lanz (1992) and by Mathys et al. (1997). We fitted three gaussians to the blend consisting of the split Fe II doublet and the unidentified rare earth line on its blue side. As stressed by Mathys et al. (1997), this represents a very effective way to disentangle the contribution of the rare earth blend from that of the two Fe II line components and to achieve consistent determinations of the wavelengths of the latter. The usage of this approach also ensures that, for a given star, the achievable precision in the measurements of  $\lambda_b$  and  $\lambda_r$  is almost independent of the spectral resolution and of the S/N of the observations acquired at different epochs, as long as both are sufficiently high. The resulting consistency in the derived values of  $\langle B \rangle$  between observations obtained at different epochs with different instrumental configurations and the uniformity of the uncertainties of these measurements are abundantly illustrated by the phase diagrams of the mean magnetic field modulus variations for numerous stars shown in Appendix A of Mathys (2017). For each star, the scatter of the measurements about a smooth variation curve is very uniform, independently of the measurement source. In other words, the adopted measurement procedure is very robust. In general, it is straightforward to ensure that all the measurements are performed in a repeatable manner, even if they were carried out years apart for different subsets of data. In only a few exceptional cases, some additional caution may be required, and achieving sufficient precision may require all the spectra of a given star to be measured in a single batch to ensure consistency. Such exceptions typically arise from the presence of an unusually strong or highly variable rare earth blend to the Fe II  $\lambda 6149.2 \text{ \AA}$  line, combined with a rather weak or very strong magnetic field. Examples include HD 965 (Mathys et al. 2019b) and HD 318107 (= CoD –32 13074 Manfroid & Mathys 2000; Mathys 2017). The case of HD 166473 is much less challenging.

Accordingly, there is no reason to expect the uncertainty of the new determinations of  $\langle B \rangle$  presented here to be significantly different from that of the previous measurements of Mathys et al. (1997), Mathys et al. (2007), and Mathys (2017). We shall see in Sect. 4 that the scatter of the measurements about the variation



**Table 2.** Mean longitudinal magnetic field measurements.

JD	$\langle B_z \rangle$ (G)	$\sigma_z$ (G)	Reference
2448782.707	-2036	105	Mathys & Hubrig (1997)
2448845.631	-2291	314	Mathys & Hubrig (1997)
2448846.696	-2110	198	Mathys & Hubrig (1997)
2449830.876	245	129	Mathys (2017)
2449916.826	711	119	Mathys (2017)
2449972.637	841	213	Mathys (2017)
2450183.873	1458	185	Mathys (2017)
2450294.775	1679	133	Mathys (2017)
2450497.889	1746	155	Mathys (2017)
2450616.882	1822	116	Mathys (2017)
2454209.827	2326	44	Bagnulo et al. (2015)
2454247.693	2298	54	Bagnulo et al. (2015)
2454250.896	2306	45	Bagnulo et al. (2015)
2454308.785	2411	45	Bagnulo et al. (2015)
2456148.655	-1218	61	This paper (HARPSpol)
2456531.773	-1741	74	This paper (ESPaDOnS)
2456547.732	-1747	69	This paper (ESPaDOnS)
2456813.014	-1495	55	This paper (ESPaDOnS)
2457239.836	-446	37	This paper (ESPaDOnS)
2457287.712	-292	45	This paper (ESPaDOnS)
2458642.993	1592	99	This paper (ESPaDOnS)

curve of the mean magnetic field modulus is fully consistent with this adopted value of the uncertainty, 80 G.

The 16 new values of the mean magnetic field modulus that we derived from the analysis of the additional spectra listed above are presented in Table 1. For the convenience of the reader, this table also includes the 40 previously published measurements. The columns give, in order, the Heliocentric (or Barycentric, for HARPS) Julian Date of mid-exposure, the value  $\langle B \rangle$  of the mean magnetic field modulus, and the instrumental configuration with which the analysed spectrum was obtained. This information had never been specified on an individual basis for some of the previously published measurements. For more detailed descriptions of the configurations used in past studies, see Mathys (2017) and references therein.

## 2.2. Mean longitudinal magnetic field

The first three measurements of the mean longitudinal magnetic field of HD 166473 were performed by Mathys & Hubrig (1997) through the analysis of spectra recorded in both circular polarisations with the ESO Cassegrain Echelle Spectrograph (CASPEC) fed by the ESO 3.6-m telescope. The value of  $\langle B_z \rangle$  was determined from the wavelength shifts of a sample of spectral lines between the two circular polarisations in each of these spectra, by application of the formula:

$$\lambda_R - \lambda_L = 2 \bar{g} \Delta \lambda_z \langle B_z \rangle, \quad (2)$$

where  $\lambda_R$  (resp.  $\lambda_L$ ) is the wavelength of the centre of gravity of the line in right (resp. left) circular polarisation and  $\bar{g}$  is the effective Landé factor of the transition.  $\langle B_z \rangle$  is determined through a least-squares fit of the measured values of  $\lambda_R - \lambda_L$  by a function of the form given above. The standard error  $\sigma_z$  that is derived from that least-squares analysis is used as an estimate of the uncertainty affecting the obtained value of  $\langle B_z \rangle$ . The same technique was subsequently applied by Mathys (2017) to obtain  $\langle B_z \rangle$  measurements at seven additional epochs from spectra recorded with the same instrument and telescope combination.

The catalogue of Bagnulo et al. (2015) lists four more values of  $\langle B_z \rangle$  in HD 166473, based on observations carried out with FORS-1 in its spectropolarimetric mode, fed by one of the Unit Telescopes of the ESO VLT. The interpretation of the FORS-1 spectropolarimetric data in terms of the mean longitudinal magnetic field, which is described in detail by Bagnulo et al. (2015), rests on assumptions and approximations that are different from those underlying Eq. (2). The  $\langle B_z \rangle$  values derived in that way may not be fully consistent with those obtained from the above-described analysis of the CASPEC data. Such disagreements between FORS-1  $\langle B_z \rangle$  measurements and determinations of this field moment through the analysis of high-resolution spectropolarimetric observations are not unusual (Landstreet et al. 2014).

To complement the  $\langle B_z \rangle$  values from the literature, here we present seven new determinations of this magnetic field moment, based on the analysis of circularly polarised spectra, one of them recorded with the polarimetric mode of HARPS at the ESO 3.6 m telescope and the other six with the ESPaDOnS spectropolarimetre (Donati et al. 2006) at the CFHT. For the latter, we used the normalised Stokes  $I$  and  $V$  spectra that are stored as telescope data products in the CFHT Archive. In the case of HARPSpol, the normalisation of the reduced spectra retrieved from the ESO Archive was carried out by Ilya Ilyin by application of the procedure described by Hubrig et al. (2013).

To ensure that the mean longitudinal magnetic field values that are determined from these spectra are as consistent as possible with the published data of Mathys & Hubrig (1997) and of Mathys (2017), we applied the following procedure. We used the same programme as these authors to measure a selected set of 20 Fe I diagnostic lines with wavelengths comprised between 5400 and 6800 Å. This is approximately the range covered by the CASPEC spectra of Mathys (2017), whose analysis was also based on a set of Fe I lines. Here, we used this same set of lines, augmented by a number of Fe I lines that were identified as suitable for the considered measurements as part of the study of Mathys & Hubrig (2006). The addition of these diagnostic lines was made possible in part by the fact that the spectral resolutions of the HARPSpol spectrum ( $R \approx 115,000$ ) and of the ESPaDOnS spectra ( $R \approx 65,000$ ) are higher than those of the CASPEC spectra ( $R \approx 18,000$  to  $39,000$ ), so that line blending is less of an issue in the former than in the latter.

All 21 values of the mean longitudinal field of HD 166473 resulting from the observations and analyses described above are listed in Table 2. The columns give, in order, the Heliocentric Julian Date of mid-observation, the value  $\langle B_z \rangle$  of the mean longitudinal magnetic field and its uncertainty  $\sigma_z$ , and the source of the measurement. For the FORS-1 measurements of Bagnulo et al. (2015), we adopted the  $\langle B_z \rangle$  values based on the analysis of the metal lines.

## 3. Variability and rotation period

To determine the rotation period of HD 166473, we fitted the measurements of its mean magnetic field modulus by a cosine wave, progressively varying the period of this wave, in search of the value of the period that minimises the reduced  $\chi^2$  of the fit. As shown in Fig. 1, the application of this procedure unambiguously indicates that the best value of the period is of the order of 3836 d.

The phase variation curve of  $\langle B \rangle$  for this value of the period is shown in Fig. 2. The time elapsed between the first determination of the mean magnetic field modulus of HD 166473 by Mathys et al. (1997) and our most recent observation of the star is 9854 d, or  $\sim 2.6$  rotation periods. The descending branch of the

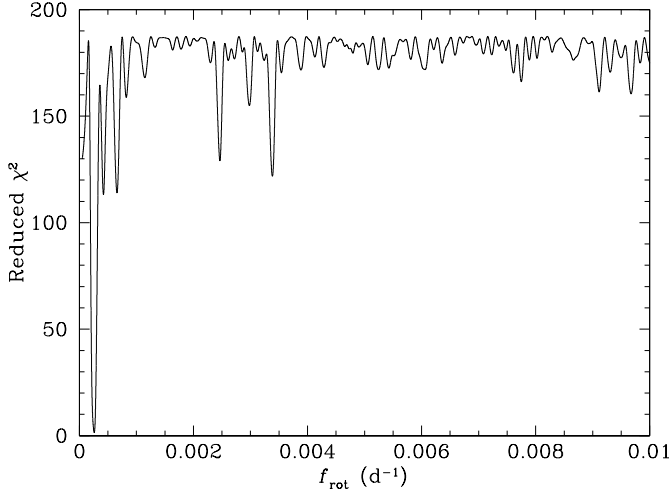


**Fig. 1.** Periodogram of the variations of the mean longitudinal magnetic field of HD 166473. The ordinate is the reduced  $\chi^2$  of a fit of the  $\langle B \rangle$  measurements by a cosine wave, with the frequency given in abscissa.

variation curve, between phases 0.05 and 0.25, is particularly interesting, as it features measurements obtained during three consecutive cycles. The data represented by circles (filled or open) are the oldest ones; the filled triangle corresponds to a measurement obtained one cycle later, and the filled squares identify observations acquired two cycles later. By increasing the trial value of the period to 3866 d, the squares are systematically shifted below the best fit curve, but within  $\sim 1\sigma$  of it. Conversely, for a trial period value of 3806 d, the squares all appear above the best fit curve, again within  $\sim 1\sigma$  of it. Outside this period range, the systematic differences between  $\langle B \rangle$  measurements from different cycles becomes too large to be accounted for only by measurement uncertainties. This constrains the uncertainty affecting the derived value of the period:

$$P_{\text{rot}} = (3836 \pm 30) \text{ d.} \quad (3)$$

The shape of the variation curve of HD 166473 appears remarkably close to a pure cosine wave (see Sect. 4), but the accuracy of the derived value of the period only depends on the reproducibility of the variation curve from cycle to cycle, regardless of its exact shape.

On the other hand, the determination of the period rests on the implicit assumption that the  $\langle B \rangle$  values that are derived from the analysis of spectra recorded with different instruments, or instrument configurations, are mutually consistent. Consideration of Fig. 2 gives strong support to the validity of this assumption. The latter is also borne out, more generically, by the overall consistency of all the  $\langle B \rangle$  measurements analysed in our recent studies of other Ap stars that rotate extremely slowly (Mathys et al. 2016; Mathys et al. 2019a; Mathys et al. 2019b). With eight different instrumental configurations used to carry out the mean magnetic field modulus measurements listed in Table 1, the consistency between all of them illustrates the robustness of the  $\langle B \rangle$  determinations obtained from the analysis of the Fe II  $\lambda 6149.2 \text{ \AA}$  line against systematic errors of instrumental origin. Exceptions certainly occur in some cases (see e.g. Mathys et al. 1997), but they are rare and their impact on the conclusions that can be drawn about the stellar physical properties from affected studies tends to be moderate.

It should be noted that the rotation period of HD 166473 is longer than the time base spanned by the magnetic measurements published by Mathys et al. (2007). The additional  $\langle B \rangle$  determinations obtained by Shavrina et al. (2014) may at most have extended this time base by a limited fraction of the rotation period, leaving its value poorly constrained in the study of these authors. Thus, our analysis provides the first accurate determination of this value.

## 4. Magnetic geometry and surface inhomogeneities

### 4.1. Magnetic variation curves

The observed variation of the mean magnetic field modulus of HD 166473 can be well represented by a cosine wave. The best least-squares fit solution for  $P_{\text{rot}} = 3836 \text{ d}$  is:

$$\begin{aligned} \langle B \rangle(\phi)[G] = & (7130 \pm 138) \\ & + (1467 \pm 19) \cos\{2\pi[\phi - (0.002 \pm 0.002)]\} \\ (\nu = 53, \chi^2/\nu = 1.5), \end{aligned} \quad (4)$$

where the field strength is expressed in Gauss,  $\phi = (\text{HJD} - \text{HJD}_0)/P_{\text{rot}} \pmod{1}$  and the adopted value of  $\text{HJD}_0 = 2448660.0$  corresponds to a maximum of the mean magnetic field modulus, within the uncertainty of the phase;  $\nu$  is the number of degrees of freedom, and  $\chi^2/\nu$ , the reduced  $\chi^2$  of the fit. The fitted curve is shown in Fig. 2; the O – C differences between the individual measurements and this curve are also illustrated. The moderate value of the reduced  $\chi^2$  is consistent with the views that the value adopted for the uncertainty affecting the derived  $\langle B \rangle$  values is realistic, and that the actual shape of the  $\langle B \rangle$  variation curve in HD 166473 is remarkably close to a pure cosine wave. This latter conclusion is particularly meaningful since the rotation cycle is sampled densely and almost uniformly by the available measurements. The scatter of the O – C data points is rather uniform and does not show any obvious systematic differences between different instrumental configurations. This justifies the adoption of a single value of the  $\langle B \rangle$  measurements errors, regardless of the spectral resolution or the S/N of the analysed spectra (see Sect. 2.1).

The sampling of the variation curve of the mean longitudinal magnetic field is sparser, with a gap of more than one third of a cycle between phases 0.60 and 0.95. Furthermore, as anticipated in Sect. 2.2, the  $\langle B_z \rangle$  values determined from FORS-1 observations that were obtained around phase 0.45 show systematic differences with respect to the  $\langle B_z \rangle$  values based on CASPEC spectra recorded around the same phase. Furthermore, we consider the CASPEC-based measurements of the mean longitudinal magnetic field from Mathys & Hubrig (1997) to be less reliable than those from Mathys (2017). Indeed, Mathys & Hubrig used transitory configurations of the CASPEC spectrograph, which were not fully characterised. Moreover, two of their measurements (represented by open squares in Fig. 3), which have higher formal errors  $\sigma_z$ , were based on spectra taken with a configuration that was used only for a single, short observing run, and spanned a shorter wavelength range than any other spectropolarimetric configuration of CASPEC. Therefore, to compute the best-fit curve that appears in Fig. 3, only the CASPEC data of Mathys (2017) were combined with the new  $\langle B_z \rangle$  measurements that we obtained from the analysis of HARPSpol and ESPaDOnS spectra. Figure 3 also includes the representative points of the  $\langle B_z \rangle$  measurements that Bagnulo et al. (2015) performed with FORS-1 and of the CASPEC data of Mathys & Hubrig (1997), but these values were not included in the computation of the fit parameters.

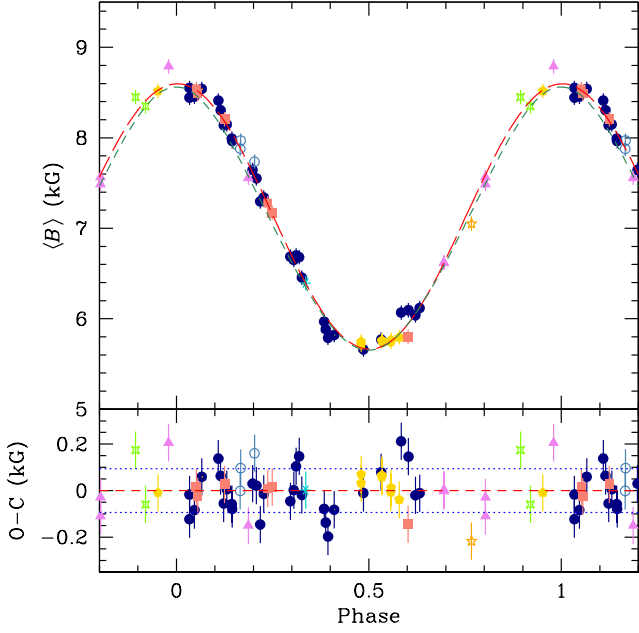


**Fig. 2.** *Upper panel:* Mean magnetic field modulus of HD 166473 against rotation phase. The different symbols identify the instrumental configuration from which the  $\langle B \rangle$  value was obtained, as follows: filled circles (dark blue): CAT + CES LC; asterisk (turquoise): CAT + CES LC, lower resolution; open circle (steel blue): CAT + CES SC; filled triangles (violet): CFHT + Gecko (all previous symbols identical to Mathys 2017); five-pointed open star (orange): 3.6 m + CES VLC; four-pointed open stars (light green): UT2 + UVES; filled pentagons (yellow): 3.6 m + HARPSpol; filled squares (salmon): CFHT + ESPaDOnS. The long-dashed line (red) is the best fit of the observations by a cosine wave – see Eq. (4). The short-dashed line (dark green) corresponds to the superposition of low-order multipoles discussed in Sect. 4. *Lower panel:* Differences O – C between the individual  $\langle B \rangle$  measurements and the best fit curve, against rotation phase. The dotted lines (blue) correspond to  $\pm 1$  rms deviation of the observational data about the fit (red dashed line). The symbols are the same as in the upper panel.

The best-fit solution that we derived is as follows:

$$\begin{aligned} \langle B_z \rangle(\phi)[G] = & (134 \pm 49) \\ & + (1798 \pm 51) \cos[2\pi [\phi - (0.540 \pm 0.005)]] \\ (\nu = 11, \chi^2/\nu = 2.3). \end{aligned} \quad (5)$$

The fit is weighted by the inverse of the square of the uncertainties of the individual measurements. The rather low value of the reduced  $\chi^2$  suggests that the measurement uncertainties are estimated correctly, that the CASPEC, HARPSpol and ESPaDOnS  $\langle B_z \rangle$  determinations are mutually consistent within these uncertainties, and that the shape of the variation curve of the mean longitudinal magnetic field modulus of HD 166473 does not differ significantly from a cosine wave. Visual inspection of Fig. 3 confirms this conclusion, and there are no indications of systematic differences between the  $\langle B_z \rangle$  values determined from the analysis of spectra taken with the three different instrumental configurations under consideration. Taking into account their higher formal errors, the measurements of Mathys & Hubrig (1997) are also consistent with the data that were included in the fit.

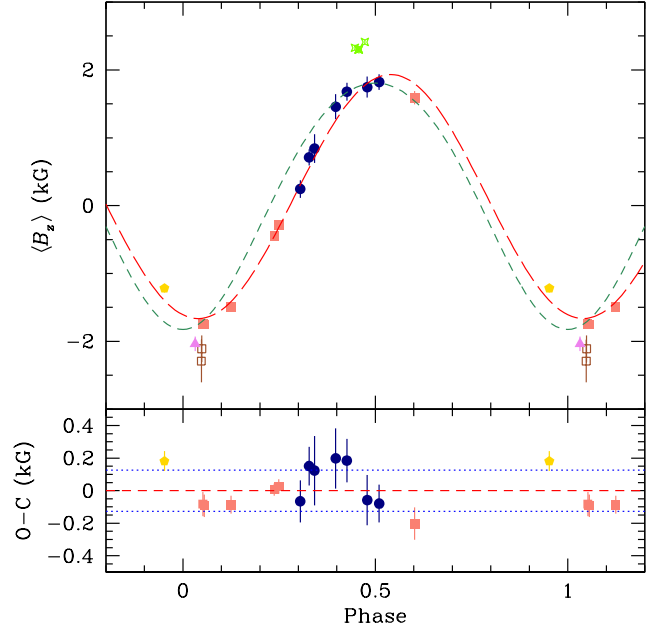


**Fig. 3.** *Upper panel:* Mean longitudinal magnetic field of HD 166473 against rotation phase. The different symbols identify the sources of the  $\langle B_z \rangle$  values, as follows: open squares (brown) or filled triangle (violet): Mathys & Hubrig (1997 CASPEC); filled circles (dark blue): Mathys (2017 CASPEC); four pointed open stars (light green): Bagnulo et al. (2015 FORS-1); filled pentagon (yellow): this paper (HARPSpol); filled squares (salmon): this paper (ESPaDOnS). The long-dashed line (red) is the best fit of the CASPEC measurements of Mathys (2017) and of the HARPSpol and ESPaDOnS data by a cosine wave – see Eq. (5). The short-dashed line (green) corresponds to the superposition of low-order multipoles discussed in Sect. 4. *Lower panel:* Differences O – C between the individual  $\langle B_z \rangle$  measurements and the best fit curve, against rotation phase. The dotted lines (blue) correspond to  $\pm 1$  rms deviation of the observational data about the fit (red dashed line). The symbols are the same as in the upper panel. The CASPEC measurements of Mathys & Hubrig (1997) and the FORS-1 measurements are not shown in this panel as they were not included in the fit (see text).

#### 4.2. Magnetic geometry

An important feature of the variation curve of the mean longitudinal magnetic field of HD 166473 is that  $\langle B_z \rangle$  undergoes sign reversals. This implies that both poles of the star come alternately into sight over a rotation cycle, a behaviour that is not predicted by the preliminary model of the magnetic field structure of HD 166473 proposed by Gerth & Glagolevskij (2003). Therefore, this model, which was only constrained by mean magnetic field modulus measurements, must be ruled out.

It is noteworthy that, to the achieved precision, which is very high for the mean magnetic field modulus, both the  $\langle B \rangle$  and  $\langle B_z \rangle$  curves are mirror-symmetric about rotation phases  $\sim 0$  and  $\sim 0.5$ . This is consistent with a magnetic field distribution that is symmetric about an axis passing through the centre of the star. However, the least-squares fits of the  $\langle B \rangle$  and  $\langle B_z \rangle$  variation curves indicate that the phases of the extrema of these two field moments are shifted with respect to each other by a small but formally significant amount. Further confirmation of



**Table 3.** Mean quadratic magnetic field measurements.

JD	$\langle B_q \rangle$ (G)	$\sigma_q$ (G)	Reference
2448782.707	9935	2091	Mathys & Hubrig (1997)
2448845.631	10774	772	Mathys & Hubrig (1997)
2448846.696	11210	573	Mathys & Hubrig (1997)
2449830.876	7434	282	Mathys (2017)
2449916.826	7556	155	Mathys (2017)
2449972.637	6482	316	Mathys (2017)
2450183.873	6840	211	Mathys (2017)
2450294.775	6630	348	Mathys (2017)
2450497.889	6188	160	Mathys (2017)
2450616.882	6183	162	Mathys (2017)
2454336.612	6849	128	This paper (HARPS)
2454338.630	6886	110	This paper (HARPS)
2454544.782	6796	112	This paper (HARPS)
2454545.866	6733	126	This paper (HARPS)
2454633.768	6770	120	This paper (HARPS)
2454634.852	6951	147	This paper (HARPS)
2454716.624	6872	122	This paper (HARPS)
2456148.655	9590	395	This paper (HARPSpol)
2456531.773	10200	130	This paper (ESPaDOnS)
2456547.732	10110	98	This paper (ESPaDOnS)
2456813.014	9709	122	This paper (ESPaDOnS)
2457239.836	9057	122	This paper (ESPaDOnS)
2457287.712	8964	161	This paper (ESPaDOnS)
2458642.993	8394	172	This paper (ESPaDOnS)

the significance of this shift needs to be sought in the future by completing the phase coverage of the  $\langle B_z \rangle$  measurements. In any event, it is considerably smaller than the shift between the  $\langle B_z \rangle$  and  $\langle B \rangle$  extrema that is observed in other super-slowly rotating Ap stars, such as HD 18078 (Mathys et al. 2016) or HD 50169 (Mathys et al. 2019a).

Comparison of the variation curves of the mean magnetic field modulus and of the mean longitudinal magnetic field definitely indicates that the field intensity is stronger over the part of the surface of the star that is seen at the phase of the negative extremum of  $\langle B_z \rangle$ , to which we shall hereafter refer to as the negative magnetic pole, than around the part of the stellar surface that is observed at the phase of the positive  $\langle B_z \rangle$  extremum (hereafter the positive pole). This represents a clear indication that, although it is nearly axisymmetric, the geometrical structure of the magnetic field of HD 166473 must depart considerably from a single dipole at the centre of the star. This conclusion is also supported by the large value of the ratio between the values of the extrema of  $\langle B \rangle$ ,  $q = 1.52$ . The latter rules out a simple dipolar field geometry, for which the maximum possible value of  $q$  is  $\sim 1.25$  (Preston 1969).

To gain more insight, it is a good approximation to try to represent the structure of the magnetic field of HD 166473 by a simple axisymmetric model, such as the superposition of collinear dipole, quadrupole and octupole (Landstreet & Mathys 2000). Through the same procedure as used by these authors, we found that the parameter values of the model that best reproduces the observations are as follows:  $i = 36^\circ \pm 3^\circ$ ,  $\beta = 90^\circ \pm 3^\circ$ ,  $B_{\text{dipole}} = (-8820 \pm 300) \text{ G}$ ,  $B_{\text{quadrupole}} = (-6580 \pm 300) \text{ G}$ , and  $B_{\text{octupole}} = (3190 \pm 300) \text{ G}$ . The variation curves of  $\langle B \rangle$  and  $\langle B_z \rangle$  that are computed with these parameters are shown in Figs. 2 and 3. This simple field model does not include the toroidal field and is only meant to obtain a preliminary estimate of the geometry of the star, that is, primarily, to constrain the inclination of the rotation axis to the line of sight (angle  $i$ ) and the angle  $\beta$  between

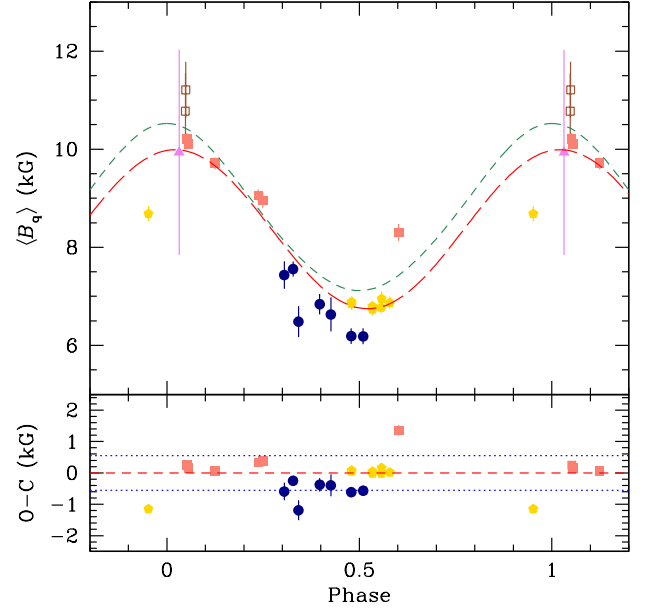


**Fig. 4.** *Upper panel:* Mean quadratic magnetic field of HD 166473 against rotation phase. The symbols have the same meaning as in Fig. 3. The long-dashed line (red) is the best fit of the CASPEC measurements of Mathys (2017) and of the HARPS and ESPaDOnS data of this paper by a cosine wave – see Eq. (6). The short-dashed line (green) corresponds to the superposition of low-order multipoles discussed in Sect. 4. *Lower panel:* Differences  $O - C$  between the individual  $\langle B_q \rangle$  measurements and the best fit curve, against rotation phase. The dotted lines (blue) correspond to  $\pm 1$  rms deviation of the observational data about the fit (red dashed line). The symbols are the same as in the upper panel. The CASPEC measurements of Mathys & Hubrig (1997) are not shown in this panel as they were not included in the fit (see text).

the magnetic axis (defined as the common axis of the collinear bipolar, quadrupolar and octupolar components of the classical poloidal field solution considered here) and the rotation axis. As usual, the angles  $i$  and  $\beta$  may be exchanged with no change in the predicted curves. It can be noted that the values derived here for these angles are not significantly different from those obtained by Landstreet & Mathys (2000), even though their preliminary model of HD 166473 was based on an estimate of the period extrapolated from observations spanning only 2300 d, and accordingly leaving a major gap in the phase coverage of the variations. Therefore, further comparison of this model with the one derived here is not meaningful.

The model parameters are valuable on a statistical basis. However, the simple representation that it provides is not meant to be physically realistic, so that the uncertainties given for the parameters are only formal. Neither should one expect this geometrical model to yield a physically meaningful magnetic map of the stellar surface. The observations that we have at our disposal until now are too incomplete and too inhomogeneous to justify an attempt at building a more realistic physical model. We plan to do so in the future, once we have acquired a complete set of data of high and uniform quality, which is in progress but whose completion still requires a few more years, given the length of the rotation period of HD 166473.

#### 4.3. Mean quadratic magnetic field

Mathys et al. (2007) and Mathys (2017) also presented measurements of the mean quadratic magnetic field  $\langle B_q \rangle$  of HD 166473, which were used by Landstreet & Mathys (2000) to constrain their tentative model, based on an assumed value of the period, of the geometric structure of the magnetic field of this star. The mean quadratic magnetic field is the square root of the sum of two field moments: (1) the average over the visible stellar disk of the square of the modulus of the magnetic vector,  $\langle B^2 \rangle$ , and (2) the average over the visible stellar disk of the square of the component of the magnetic vector along the line of sight,  $\langle B_z^2 \rangle$ . Both averages are weighted by the local emergent line intensity.

As part of the analysis of the HARPSpol and ESPaDOnS spectra that was carried out to determine the mean longitudinal magnetic field, we also derived values of the mean quadratic magnetic field. Additional determinations of this field moment were carried out from the HARPS spectra recorded in natural light from which  $\langle B \rangle$  measurements were obtained (see Sect. 2.1). The resulting fourteen newly derived values of  $\langle B_q \rangle$  are presented in Table 3, together with the ten measurements that had been previously published. The columns give, in order, the Heliocentric Julian Date of mid-observation, the value  $\langle B_q \rangle$  of the mean quadratic magnetic field and its uncertainty  $\sigma_q$ , and the source of the measurement. The corresponding phase diagram is shown in Fig. 4.

The determination of  $\langle B_q \rangle$  from the HARPS and ESPaDOnS spectra was carried out as described in detail by Mathys (2017). In particular, we took advantage of the availability of six ESPaDOnS spectra obtained with the same configuration to derive the non-magnetic contributions to the second-order moments of the Stokes  $I$  line profiles from consideration of the average of the profiles at the six epochs of observation. The same approach was applied to the eight HARPS observations.

The determination of the mean quadratic magnetic field involves a multiple linear regression analysis to untangle the contributions of various broadening effects to the overall Stokes  $I$  line widths, as measured by the second-order moments of their profiles about their centres. As noted by Mathys & Hubrig (2006), the achievable precision on the derived value of  $\langle B_q \rangle$  may be limited by the occurrence of some crosstalk between the Doppler and Zeeman terms of the regression equation. The Doppler term includes the contribution of the instrumental profile, which depends on the spectral resolution. This may lead to systematic differences between the values of  $\langle B_q \rangle$  that are determined from spectra obtained with different instruments. Mathys (2017) reports that the values  $\langle B_q \rangle$  that he derives from CASPEC spectra ( $R \approx 39,000$ ) are not fully consistent with the values obtained from EMMI spectra ( $R \approx 70,000$ ) by Mathys & Hubrig (2006), for some stars in common. The consideration of Fig. 4 suggests that there may also be systematic differences between the quadratic field determinations carried out with each of the three instruments: CASPEC, HARPS and ESPaDOnS. In particular, the ESPaDOnS data point at phase 0.6 seems inconsistent with the CASPEC and HARPS measurements in the phase range 0.3–0.6. The HARPS determination at phase 0.95 also seems difficult to reconcile with the CASPEC and ESPaDOnS field values from the phase interval 0.0–0.1. These systematic effects appear all the more likely since the observations with each of the three instruments sample different parts of the stellar rotation cycle, which are characterised by very different values of the mean magnetic field modulus. That the crosstalk between the Doppler and Zeeman terms of the regression equation is different in these three phase intervals seems very plausible. Since there are

no other stars until now for which sets of  $\langle B_q \rangle$  measurements have been obtained with CASPEC, HARPS and ESPaDOnS, we cannot draw further conclusions about the possible different systematic effects that may affect the determinations of the mean quadratic magnetic field with these three instruments.

Accordingly, we do not believe that the different sets of mean quadratic magnetic field measurements available for HD 166473 can be reliably combined to constrain the geometrical structure of the magnetic field of this star. Therefore, we computed a fit of the variation of  $\langle B_q \rangle$  by a cosine wave only for illustrative purposes:

$$\begin{aligned} \langle B_q \rangle(\phi) = & (8368 \pm 125) \\ & + (1621 \pm 146) \cos\{2\pi[\phi - (0.022 \pm 0.023)]\} \\ & (\nu = 18, \chi^2/\nu = 10.7). \end{aligned} \quad (6)$$

This fit, which is weighted by the inverse of the square of the uncertainties of the individual measurements, is based on the CASPEC data from Mathys (2017) and on the HARPS and ESPaDOnS  $\langle B_q \rangle$  determinations of this paper. The value of the reduced  $\chi^2$  is somewhat high, which lends support to the suspicion that the mean quadratic magnetic field values derived from spectra taken with the different instruments may not be fully consistent. The consideration of the distribution of the data points about the best-fit curve in Fig. 4 further strengthens this interpretation. It should be noted that the addition of the first harmonic to the fitted function does not improve the quality of the fit. Figure 4 also shows the  $\langle B_q \rangle$  variation curve predicted by the simple multipolar model discussed above. The model provides a rough but reasonable approximation of the observed variations of the quadratic field, whether or not the measurements of this field moment are used to constrain it. In particular, that the model curve tends to be shifted towards higher values with respect to the measurements is not inconsistent with the observation that, frequently, the derived values of  $\langle B_q \rangle$  tend to slightly underestimate the actual magnetic field (Mathys & Hubrig 2006; Mathys 2017).

#### 4.4. Line intensity variations

With the diversity of instrumental configurations used for the determination of the mean magnetic field modulus, only a narrow wavelength range is common to all the recorded spectra. A segment of this common range is shown in Fig. 5. It includes two of the few spectral lines in this region that appear reasonably free from blends: Nd III  $\lambda 6145$  Å and Fe II  $\lambda 6147.7$  Å. These two lines show significant variations with rotation phase, as can be seen in Figs. 7 and 8. Both lines are strong: the overabundance of the Rare Earth Elements and the moderate enhancement of the iron-peak elements in the photosphere of HD 166473 were first reported by Gelbmann et al. (2000). In hotter Ap stars, the latter line arises almost entirely from a Fe II transition of the same multiplet 74 as Fe II  $\lambda 6149.2$  Å. However, in cool stars such as HD 166473, it also includes a significant contribution from a Fe I line at 6147.8 Å (Mathys & Lanz 1992). This does not represent an issue, as the horizontal distributions of Fe I and Fe II over the surface of Ap stars are in general identical. While there may also be a small contribution of the Ti I  $\lambda 6147.76$  transition, the main element responsible for the observed line at 6147.7 Å and its variations is undoubtedly Fe. At the field strengths present in HD 166473, magnetic desaturation of the spectral lines is almost complete, so that the observed line intensity variations cannot be assigned to differences in magnetic line intensification between different parts of the stellar surface. Instead, they must reflect the



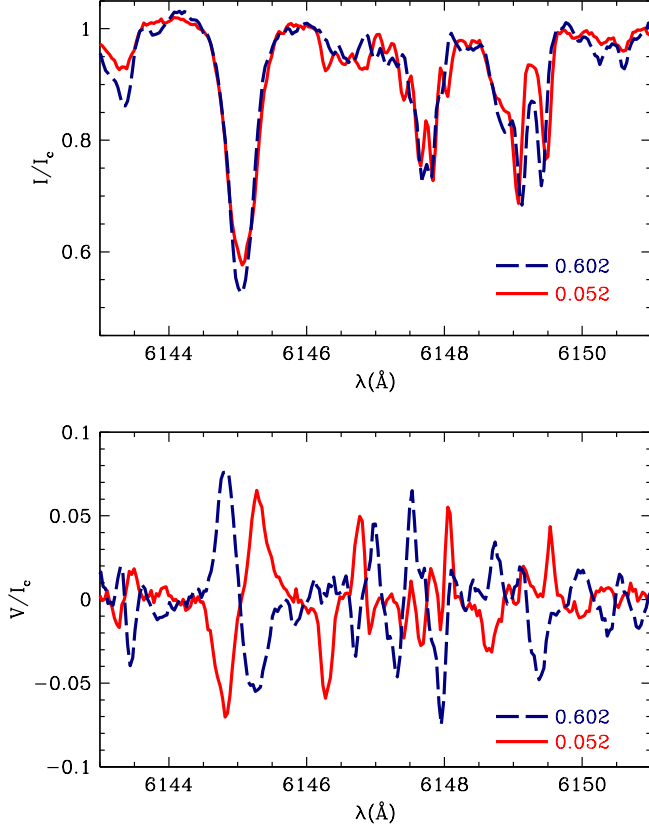


**Fig. 5.** Part of the region of the spectrum of HD 166473 that is common to all the high-resolution spectra from which the mean magnetic field modulus measurements of Table 1 were obtained. Stokes  $I$  (upper panel) and Stokes  $V$  (lower panel) spectra, recorded at phases 0.052 (solid red line) and 0.602 (dashed blue line) are shown; they are normalised to the local unpolarised continuum intensity  $I_c$ . The main lines are Nd III  $\lambda$  6145 Å (not fully resolved), Fe II  $\lambda$  6147.7 Å (with a quadruplet pattern), and Fe II  $\lambda$  6149.2 Å (a doublet, blended on the blue side with an unidentified rare earth line).

existence of horizontal abundance inhomogeneities across this surface.

The Stokes  $I$  and  $V$  spectra shown in Fig. 5 were obtained with ESPaDOnS close to the phases of the magnetic extrema. The Stokes  $V$  plot clearly illustrates the reversal of the mean longitudinal magnetic field. In the Stokes  $I$  tracings, one can easily see the greater wavelength separation of the split components of the resolved lines close to phase 0 than to phase 0.5.

The same observations can also be plotted in a different form, showing the Stokes  $I + V$  and  $I - V$  spectra at the two phases of interest (see Fig. 6), to emphasise the polarisation of the individual split line components. This is illuminating, in particular for the outermost  $\sigma$  components of the Fe II  $\lambda$  6147.7 Å quadruplet at phase 0.602: the blue one is almost fully circularly polarised to the left, and the red one is almost fully circularly polarised to the right. (For a detailed description of the Zeeman pattern of the Fe II  $\lambda$  6147.7 Å transition, see Mathys 1990.) The polarisations of these components are swapped, but less complete at phase 0.052. This is an indication of the presence of mixed field polarities on the stellar hemisphere that is visible around

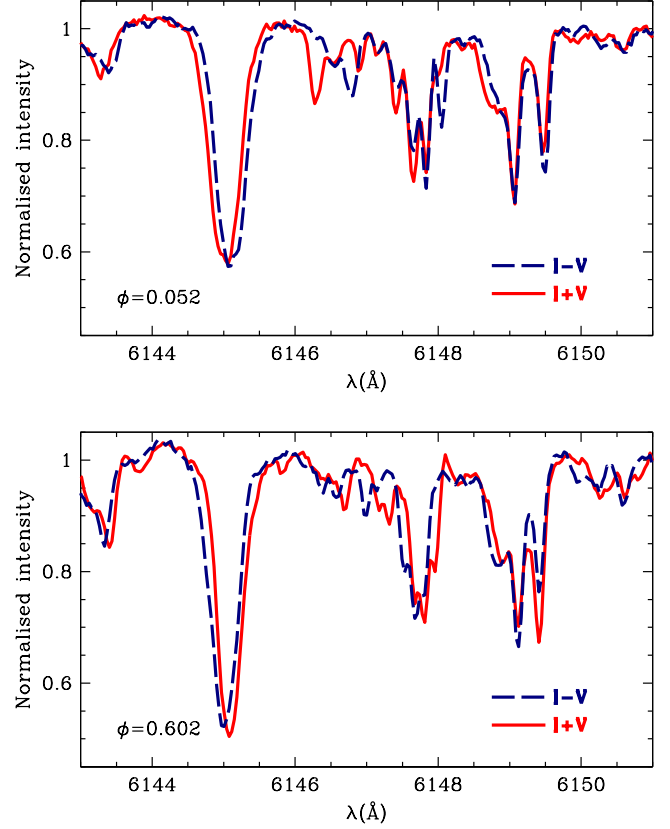


**Fig. 6.** Part of the region of the spectrum of HD 166473 that is common to all the high-resolution spectra from which the mean magnetic field modulus measurements of Table 1 were obtained. Spectra recorded at phases 0.052 (upper panel) and 0.602 (lower panel) are shown, in right circular polarisation ( $I + V$ ; solid red line) and in left circular polarisation ( $I - V$ ; dashed blue line). The main lines are Nd III  $\lambda$  6145 Å (not fully resolved), Fe II  $\lambda$  6147.7 Å (with a quadruplet pattern), and Fe II  $\lambda$  6149.2 Å (a doublet, blended on the blue side with an unidentified rare earth line).

phase 0, while no field polarity change should occur over most of the hemisphere that is observed around phase 0.5. We expect to be able to confirm and fully characterise this through the detailed physical modelling that we plan to carry out once we have acquired spectra of the required quality with the necessary phase sampling (see Sect. 4.2). The simple geometrical model presented here is unsuitable for such an endeavour.

The variation curves of the equivalent widths of the lines Nd III  $\lambda$  6145 Å (Fig. 7) and Fe II  $\lambda$  6147.7 Å (Fig. 8) both show two maxima and two minima per rotation cycle. The maxima occur close to the phases of extrema of the magnetic field moments: that is, both lines are stronger in the vicinity of the magnetic poles. The Nd III  $\lambda$  6145 Å line is significantly stronger close to the positive pole than to the negative one, while the Fe II  $\lambda$  6147.7 Å line seems rather stronger close to the negative pole. The two equivalent widths minima, for each of the two lines, also appear to differ from each other. This points at a non-axisymmetric distribution of the elemental abundances over the surface of HD 166473, despite the plausibly axisymmetric structure of the magnetic field. This should not be regarded as a major

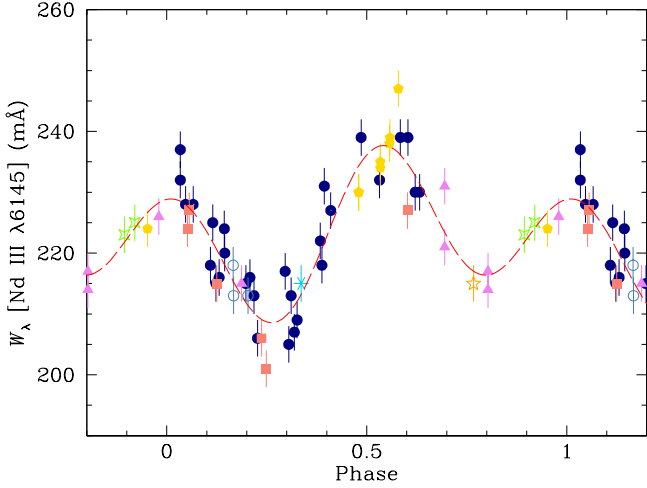


**Fig. 7.** Equivalent width of the Nd III  $\lambda 6145$  Å line against rotation phase. The symbols have the same meaning as in Fig. 2. The long-dashed line (red) is the best fit of the measurements by a cosine wave and its first harmonic. It has been included to guide the eye despite its lack of physical meaning.

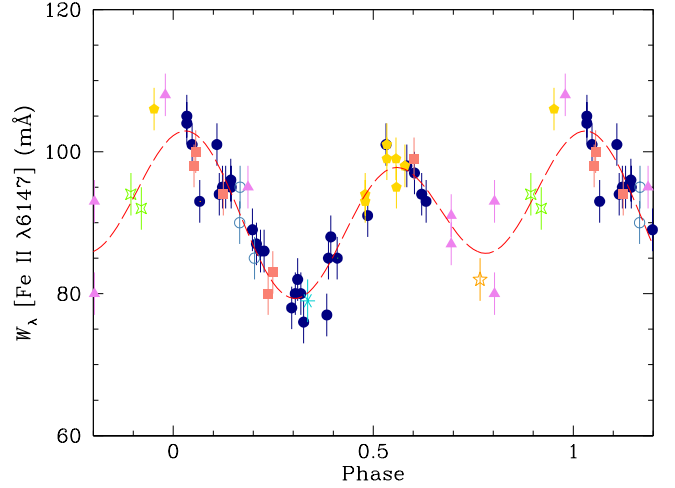


**Fig. 8.** Equivalent width of the Fe II  $\lambda 6147$  Å line against rotation phase. The symbols have the same meaning as in Fig. 2. The long-dashed line (red) is the best fit of the measurements by a cosine wave and its first harmonic. It has been included to guide the eye despite its lack of physical meaning.

discrepancy, since contrary to what has been assumed for a long time, the distribution of elemental abundances on the surfaces of the Ap stars may show only loose correlations (or none at all) with the magnetic structure (e.g., Rusomarov et al. 2018).

On the other hand, Fe lines were used for the measurements of the mean magnetic field modulus and of the mean longitudinal magnetic field from which we computed a model of the structure of the field. Accordingly, the geometry that we derived is actually a convolution of the actual structure of the magnetic field with the distribution of the Fe line intensity across the star. Untangling these two components would require elaborate numerical modelling beyond the scope of the present study, for which the observational data used in this analysis are insufficient. Moreover, it is unclear to which extent and how uniquely the untangling of the magnetic geometry and of the elemental abundance distribution could be achieved since, in contrast with Ap stars with rotation periods not exceeding a few weeks, there is no significant rotational Doppler effect to shift the contributions of regions of the stellar surface of different longitudes with respect to each other in the observed, disk-integrated spectral line profiles.

## 5. Discussion

Following this study, HD 166473 becomes only the fourth Ap star with a rotation period longer than 10 years for which magnetic field measurements have been obtained over more than a full cycle. With the addition of HD 166473, there are now eight Ap stars for which rotation periods longer than 1000 d have been accurately determined and magnetic variations have been well sampled over a full rotation period. These stars are listed, in order of decreasing period, in Table 4. The columns give, in order: the HD number of the star, another identification, the spectral type according to Renson & Manfroid (2009), the rotation period, the reference from which it is extracted, the rms mean longitudinal field  $\langle B_z \rangle_{\text{rms}}$  (as defined by Bohlender et al. 1993), the average over a rotation cycle of the mean magnetic field modulus ( $B_0$ ), the ratio of  $\langle B_z \rangle_{\text{rms}}$  to  $B_0$ , the ratio  $q$  of the extrema of the

mean magnetic field modulus, the ratio  $r$  of the smaller (in absolute value) to the larger (in absolute value) extremum of  $\langle B_z \rangle$ , and some notes (SB1 and SB2 identify, respectively, single-lined and double-lined spectroscopic binaries). Most information for each star was extracted or computed from the sources from which the values of the periods were retrieved, and from the references quoted in these sources. For HD 9996 and HD 187474, additional magnetic field measurements from Mathys (2017) were included in the computation of the magnetic parameters.

The  $\langle B_z \rangle$  measurements from the quoted references were used to compute the values of  $\langle B_z \rangle_{\text{rms}}$  that appear in Table 4. Although possible in principle, determining the mean longitudinal magnetic fields of stars in SB2 systems is considerably less straightforward than in single stars. This has not been done yet in a systematic way for HD 59435.

For each star, the value that is given for the average of the mean magnetic field modulus over a rotation cycle is that of the independent term  $B_0$  of the least-squares fit of the  $\langle B \rangle$  measurements by a cosine wave, or by a cosine wave and its first harmonic, as adopted in the quoted reference. This value is undefined for HD 9996, since its spectrum only shows resolved lines over a small fraction ( $\sim 0.3$ ) of its rotation cycle (Mathys 2017). Outside this phase interval,  $\langle B \rangle$  cannot be determined. However, for most of the cycle, its value must be considerably less than 3.5 kG. Accordingly, the ratio  $q$  between the extrema of the mean magnetic field modulus of HD 9996 may plausibly be close to 2.0, which is approximately the largest value observed in any Ap star for which the  $\langle B \rangle$  variation curve is fully constrained. In this case,  $B_0$  could be of the order of 3.8 kG, since the highest value of  $\langle B \rangle$  that has been measured in HD 9996 is  $\sim 5.1$  kG.

Among the stars of Table 4, HD 166473 has the strongest mean magnetic field modulus, as characterised by its average value over a rotation cycle,  $B_0 = 7131$  G. This value is close to, but below, the 7.5 kG value that seems to represent an upper limit to the field strengths for Ap stars that rotate extremely slowly ( $P_{\text{rot}} \gtrsim 150$  d; Mathys et al. 1997; Mathys 2017). As mentioned in Sect. 1, among the roAp stars, HD 154708 definitely has a stronger magnetic field than HD 166473. The case of HD 92499 is less clearcut, as only a few measurements of its

**Table 4.** Ap stars with accurately determined rotation periods longer than 1000 d.

HD	Other id.	Sp. type	$P_{\text{rot}}$ (d)	Ref.	$\langle B_z \rangle_{\text{rms}}$ (G)	$B_0$ (G)	$\langle B_z \rangle_{\text{rms}}/B_0$	$q$	$r$	Notes
50169	BD −1 1414	A3p SrCrEu	10600	1	1294	5076	0.25	1.43	−0.96	SB1
9996	HR 465	B9p CrEuSi	7937	2	713	—	—	—	−0.35	SB1
965	BD −0 21	A8p SrEuCr	6030	3	775	4253	0.18	1.00	−0.50	
166473	CoD −37 12303	A5p SrEuCr	3836	4	1682	7131	0.24	1.52	−0.99	roAp
94660	HR 4263	A0p EuCrSi	2800	5	1911	6232	0.31	1.06	0.92	SB1
187474	HR 7552	A0p EuCrSi	2345	6	1470	5417	0.27	1.27	−0.98	SB1
59435	BD −8 1937	A4p SrCrEu	1360	7	—	3036	—	1.87	—	SB2
18078	BD +55 726	A0p SrCr	1358	8	692	3450	0.20	1.81	−0.92	SB1

**References.** (1) Mathys et al. (2019a); (2) Bychkov et al. (2012); (3) Mathys et al. (2019b); (4) This paper; (5) Mathys (2017); (6) Mathys (1991); (7) Wade et al. (1999); (8) Mathys et al. (2016).

mean magnetic field modulus have been obtained, and its variation is not well characterised. The  $\langle B \rangle$  values that have been determined for this star at various epochs (Hubrig & Nesvacil 2007; Freyhammer et al. 2008; Elkin et al. 2010), which range from 8.2 to 8.5 kG, are greater than the average value of the mean magnetic field modulus of HD 166473 over its rotation cycle,  $B_0 = 7.1$  kG, but they do not exceed its value at the phase of maximum, 8.6 kG. The average value of  $\langle B \rangle$  over the rotation cycle of HD 92499, and how it compares with HD 166473, is still unknown. Notwithstanding, HD 166473 is definitely one of the most strongly magnetic roAp stars. Moreover, it is at present the only roAp star with a rotation period longer than 1000 d for which the accurate value of this period has been determined and the magnetic variations have been fully characterised. However, several other roAp stars definitely have rotation periods of several years, which the observations that have been obtained until now do not cover entirely yet.

Within the framework of the extensive, parameter-based, statistical study of Mathys (2017), HD 166473 does not stand out as particularly remarkable in any respect. The ratios  $q$  and  $r$  of the extrema of its mean magnetic field modulus and of its mean magnetic longitudinal field, and the relation between the averages of these field moments over a rotation cycle as characterised by the ratio  $\langle B_z \rangle_{\text{rms}}/B_0$ , are within the typical ranges (Mathys 2017). That the variation curves of  $\langle B \rangle$  and of  $\langle B_z \rangle$  show no significant departure from harmonicity differentiates HD 166473 from the other stars of Table 4, except maybe HD 965 (for which no significant variation of  $\langle B \rangle$  is detected). However, such a behaviour is rather common in shorter period stars (Mathys 2017). Moreover, the phase difference (0.538) between the cosine fits to the  $\langle B_z \rangle$  and  $\langle B \rangle$  measurements is well within one of the “normality” bands of Fig. 11 of Mathys (2017).

More generally, consideration of Table 4 as a whole is intriguing in several respects. First of all, the spectral types of the stars in this table range from B9p to A8p, encompassing most of the temperature interval in which classical Ap stars are found, except for its lower end. This is rather surprising, at it is generally accepted that lower mass and lower temperature Ap stars rotate in average slower than their more massive, hotter counterparts (see Fig. 6 of Netopil et al. 2017). One would rather expect the majority of the most slowly rotating Ap stars to have late A or early F spectral types. That this is not the case for those extremely long period Ap stars of which a full rotation cycle has been covered by the observations obtained until now may be coincidental, due to the small number of these stars. The same explanation probably accounts for the high fraction of spectro-

scopic binaries in Table 4. Indeed, out of the eight stars listed in this table, six are spectroscopic binaries. This represents a fraction considerably greater than the overall rate of occurrence of binarity among Ap stars, which is of the order of 50% according to the most recent estimates (Mathys 2017 and references therein). All the binaries listed in Table 4 have orbital periods of several hundred days (for their exact values, see Mathys 2017), so that tidal interaction between the components must be negligible.

However, the most significant feature of Table 4 may be the distribution of the values of the ratio  $r$  between the extrema of the mean longitudinal magnetic field. It is remarkable that  $r < -0.90$  for half the stars of this table, and that  $r < 0.00$  for all of them but HD 94660. Although measurements of  $\langle B_z \rangle$  covering a full rotation cycle have not been obtained for HD 59435, and no individual values have been published, the range covered by the existing measurements, as reported by Romanyuk & Kudryavtsev (2008), definitely indicates that  $r$  is negative. The distribution of the values of  $r$  in Table 4 can be compared with their distribution for the Ap stars with resolved magnetically split lines for which  $\langle B_z \rangle$  measurements well distributed over a rotation cycle are available, as listed in Tables 13 and 14 of Mathys (2017). Excluding the stars also listed in Table 4 of the present paper, these two tables contain 6 stars for which  $r < 0$  and 18 stars for which  $r > 0$ . The rotation periods of all of them are shorter than 1000 d. For only one of them, HD 200311,  $r < -0.90$ . Even though caution is still called for about the statistical significance of the conclusions that can be drawn from a sample of only eight well studied Ap stars with  $P_{\text{rot}} > 1000$  d, the contrast in the rates of occurrence of negative values of  $r$ , especially large ones, between this group and the shorter period stars from the sample of Mathys (2017), is striking. Large (in absolute value) negative values of  $r$  are indicative of values close to  $90^\circ$  of one of the angles  $i$  or  $\beta$ . There is no reason to expect any difference between the stars with periods longer or shorter than 1000 d in the distribution of the inclination angles  $i$  of the rotation axes to the line of sight. Thus, any difference in the distribution of the  $r$  values between the two groups must arise from different distributions of the inclination of the magnetic axes with respect to the rotation axes. Specifically, the high rate of occurrence of mostly large negative values of  $r$  in Table 4 strongly suggests that the angle between the magnetic and rotation axes systematically tends to be large in the most slowly rotating Ap stars. The existence of such a trend was already proposed by Mathys (2017). The evidence presented here strengthens the case.



With the growing number of extremely slowly rotating Ap stars whose periods have been accurately determined and whose magnetic field variations have been fully characterised over a full cycle, there is little doubt left that, on an individual basis, these stars do not distinguish themselves from faster rotating Ap stars in any other respect. However, they may as a group have properties that differentiate them from other subgroups of Ap stars. In this respect, one of the most intriguing possibilities to which the available evidence seems to point, albeit with limited statistical significance, is a tendency for the angle between the magnetic and rotation axes to be systematically large. Other aspects that deserve further investigation include the rate of occurrence of extremely slowly rotating Ap stars in binary systems, the confirmation and, possibly, the further characterisation of the apparent lack of very strong magnetic fields in the longest period Ap stars, and the possible mass dependence of the occurrence of super slow rotation. Knowledge of these various aspects and of the constraints that they imply is essential for progress in the understanding of the formation and evolution of the Ap stars and of their magnetic fields. Therefore, it is critically important to acquire on a regular basis new observations of the most slowly rotating Ap stars with a view to building a set of such stars, whose rotation period is accurately determined and whose magnetic field is fully characterised, that is sufficiently populated to allow statistically significant conclusions to be derived reliably.

*Acknowledgements.* We thank the anonymous referee for calling our attention to the availability of the HARPSpol observation of HD 166473 in the ESO Archive, and for thought-provoking comments. We also thank Svetlana Hubrig and Ilya Ilyin for providing the normalised version of these reduced HARPSpol spectra that were used in this analysis. VK and JDL acknowledge support from the Natural Sciences and Engineering Research Council of Canada.

## References

- Bagnulo, S., Fossati, L., Landstreet, J. D., & Izzo, C. 2015, A&A, 583, A115  
 Bohlender, D. A., Landstreet, J. D., & Thompson, I. B. 1993, A&A, 269, 355  
 Bychkov, V. D., Bychkova, L. V., Madej, J., & Shatilov, A. V. 2012, Acta Astron., 62, 297  
 Dall, T. H. 2005, CES Users Manual, Issue 1.3, ESO  
 Donati, J.-F., Catala, C., Landstreet, J. D., & Petit, P. 2006, in Solar Polarization 4, Vol. 358, 362  
 Donati, J.-F., Semel, M., Carter, B. D., Rees, D. E., & Collier Cameron, A. 1997, MNRAS, 291, 658  
 Elkin, V. G., Kurtz, D. W., Mathys, G., & Freyhammer, L. M. 2010, MNRAS, 404, L104  
 Freyhammer, L. M., Elkin, V. G., Kurtz, D. W., Mathys, G., & Martinez, P. 2008, MNRAS, 389, 441  
 Gelbmann, M., Ryabchikova, T., Weiss, W. W., et al. 2000, A&A, 356, 200  
 Gerth, E. & Glagolevskij, Y. V. 2003, Bulletin of the Special Astrophysics Observatory, 56, 25  
 Hubrig, S., Ilyin, I., Schöller, M., & Lo Curto, G. 2013, Astronomische Nachrichten, 334, 1093  
 Hubrig, S., Järvinen, S. P., Madej, J., et al. 2018, MNRAS, 477, 3791  
 Hubrig, S. & Nesvacil, N. 2007, MNRAS, 378, L16  
 Khalack, V., Gallant, G., & Thibault, C. 2017, MNRAS, 471, 926  
 Kurtz, D. W., Elkin, V. G., Cunha, M. S., et al. 2006, MNRAS, 372, 286  
 Kurtz, D. W., Elkin, V. G., & Mathys, G. 2003, MNRAS, 343, L5  
 Kurtz, D. W. & Martinez, P. 1987, MNRAS, 226, 187  
 Landstreet, J. D., Bagnulo, S., & Fossati, L. 2014, A&A, 572, A113  
 Landstreet, J. D. & Mathys, G. 2000, A&A, 359, 213  
 Manfroid, J. & Mathys, G. 2000, A&A, 364, 689  
 Mathys, G. 1990, A&A, 232, 151  
 Mathys, G. 1991, A&AS, 89, 121  
 Mathys, G. 2017, A&A, 601, A14  
 Mathys, G. & Hubrig, S. 1997, A&AS, 124, 475  
 Mathys, G. & Hubrig, S. 2006, A&A, 453, 699  
 Mathys, G., Hubrig, S., Landstreet, J. D., Lanz, T., & Manfroid, J. 1997, A&AS, 123, 353  
 Mathys, G., Kurtz, D. W., & Elkin, V. G. 2007, MNRAS, 380, 181  
 Mathys, G. & Lanz, T. 1992, A&A, 256, 169  
 Mathys, G., Romanyuk, I. I., Hubrig, S., et al. 2019a, A&A, 624, A32  
 Mathys, G., Romanyuk, I. I., Hubrig, S., et al. 2019b, A&A, 629, A39  
 Mathys, G., Romanyuk, I. I., Kudryavtsev, D. O., et al. 2016, A&A, 586, A85  
 Netopil, M., Paunzen, E., Hümmerich, S., & Bernhard, K. 2017, MNRAS, 468, 2745  
 Piskunov, N., Snik, F., Dolgoplov, A., et al. 2011, The Messenger, 143, 7  
 Preston, G. W. 1969, ApJ, 158, 1081  
 Pyper, D. M. & Adelman, S. J. 2017, PASP, 129, 104203  
 Renson, P. & Manfroid, J. 2009, A&A, 498, 961  
 Romanyuk, I. I. & Kudryavtsev, D. O. 2008, Astrophysical Bulletin, 63, 139  
 Rusomarov, N., Kochukhov, O., & Lundin, A. 2018, A&A, 609, A88  
 Shavrina, A. V., Khalack, V., Glagolevskij, Y., et al. 2014, in Magnetic Fields throughout Stellar Evolution, Vol. 302, 274–275  
 Smalley, B., Niemczura, E., Murphy, S. J., et al. 2015, MNRAS, 452, 3334  
 Sugar, J. & Corliss, C. 1985, Atomic energy levels of the iron-period elements: Potassium through Nickel (Washington: American Chemical Society)  
 Wade, G. A., Mathys, G., & North, P. 1999, A&A, 347, 164